CHEMISTRY OF MATERIALS

Article

pubs.acs.org/cm

Interaction of Acid Gases SO_2 and NO_2 with Coordinatively Unsaturated Metal Organic Frameworks: M-MOF-74 (M = Zn, Mg, Ni, Co)

Kui Tan,[†] Sebastian Zuluaga,[‡] Hao Wang,[§] Pieremanuele Canepa,[‡,§] Karim Soliman,[‡] Jeremy Cure,[†] Jing Li,[∥] Timo Thonhauser,[‡,⊥] and Yves J. Chabal*[,†]

[†]Department of Materials Science & Engineering, University of Texas at Dallas, Richardson, Texas 75080, United States

[‡]Department of Physics, Wake Forest University, Winston-Salem, North Carolina 27109, United States

[§]Materials Science Division, Lawrence Berkeley National Laboratory, Berkeley, California 94720, United States

[∥]Department of Chemistry and Chemical Biology, Rutgers University, Piscataway, New Jersey 08854, United States

[⊥]Department of Chemistry, Massachusetts Institute of Technology, Cambridge, Massachusetts 02139, United States

Supporting Information

ABSTRACT: *In situ* infrared spectroscopy and *ab initio* density functional theory (DFT) calculations are combined to study the interaction of the corrosive gases SO_2 and NO_2 with metal organic frameworks M-MOF-74 (M = Zn, Mg, Ni, Co). We find that NO_2 dissociatively adsorbs into MOF-74 compounds, forming NO and NO_3^-. The mechanism is unraveled by considering the Zn-MOF-74 system, for which DFT calculations show that a strong NO_2−Zn bonding interaction induces a significant weakening of the N−O bond, facilitating the decomposition of the NO_2 molecules. In contrast, SO_2 is only molecularly adsorbed into MOF-74 with high binding energy (>90 kJ/mol for Mg-MOF-74 and >70 for Zn-MOF-74). This work gives insight into poisoning issues by minor components of flue gases in metal organic frameworks materials.

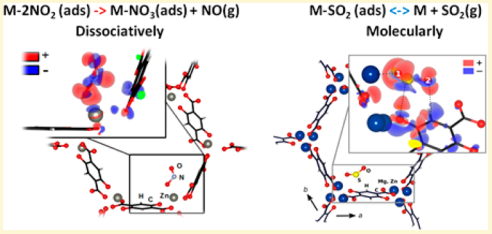

1. INTRODUCTION

Metal organic frameworks (MOFs) are porous materials that have attracted a great deal of attention in the past decade for a variety of applications such as gas adsorption, storage, separation, and catalysis.[1−9] Their structure is composed of metal ions or clusters as the node and organic molecules as the bridge to form one, two, or three dimension open networks that can accommodate a variety of guest molecules. One promising application is the capture of CO_2 by MOFs from power plant flue gas streams.[8,10] In the past few years, there has been a great deal of effort to design and prepare MOF structures with higher affinity and selectivity toward CO_2 over other components such as N_2 and O_2,[11−16] such as the incorporation of coordinatively unsaturated metal sites binding sites into the frameworks structure to obtain higher energy. MOF-74 [M_2(dhtp), M = Mg, Zn, Ni, Co^{2+} and dhtp = 2,5-dihydroxyterephthalate] compounds represent the best example containing a high density of coordinatively unsaturated open metal sites that interact strongly with CO_2 and have the highest CO_2 uptake capacity at flue gas partial pressure ∼0.1 bar.[17−20]

Although MOFs have great potential to separate CO_2 from flue gas mixtures, some considerations must be taken into account for evaluating the performance in real-world applications. One issue is that flue gas impurities such as the corrosive acid gases sulfur oxides SO_x (mainly SO_2) and nitrogen oxides NO_x (mainly NO, NO_2) could adsorb into MOFs and potentially poison the materials by reacting with or strongly bonding to the active sites.[8] Some theoretical work has recently been done to examine the adsorption of trace flue gas contaminants (SO_2, NO_2, NO) in M-MOF-74 (M = Mg, Ni, Co) compounds.[21−24] For example, Schmidt[21] and co-worker's density functional theory (DFT) calculations of different species (SO_2, SO_3, NO, NO_2) adsorption in Mg-MOF-74 suggest that SO_2 could be a potentially serious poison for Mg-MOF-74 because of its high binding strength (72.8 kJ/mol) at the open metal sites within the structure. Furthermore, hydrate acids such as H_2SO_3 and H_2SO_4 may form and bind extremely strongly (exceeding 100 kJ/mol) and saturating nearly all available metal sites.[21] In contrast to SO_2, NO_2, and NO molecules are characterized by modest binding energies (41.3 kJ/mol for NO_2 and 33.2 kJ/mol for NO) similar to that of CO_2. It was therefore believed that NO_x species are less serious poisons than SO_x molecules. This difference in binding energies was consistent with Ding's and Neaton's calculations.[22,25,26] These molecular adsorption studies provided the initial ideas of the possible interaction of NO_x and SO_x with MOFs. However, these acid gas molecules are likely to have a complex interaction

Received: January 6, 2017
Revised: April 29, 2017
Published: May 1, 2017

DOI: 10.1021/acs.chemmater.7b00005
Chem. Mater. 2017, 29, 4227−4235

with surfaces, with strong temperature dependence, due to the high reactivity of the SO_x and NO_x species. For instance, different species such as NO, NO_2^-, NO_3^-, SO_3^{2-}, and SO_4^{2-} are formed on metal or metal oxides surfaces such as MgO and ZnO upon NO_2 and SO_2 adsorption.[27−31] Calculations show that the exposed metal and oxygen sites on the oxide surfaces are the reactive centers for NO_2 and SO_2, respectively. Based on these considerations, NO_2 and SO_2 might exhibit a rich chemistry rather than being only molecularly adsorbed into the M-MOF-74 (M = Zn, Mg, Ni, Co) as investigated by the above-mentioned studies. Therefore, it is worthwhile to experimentally examine the interaction of SO_2 and NO_2 with MOF-74.

In the present work, *in situ* infrared spectroscopy and first principle calculations are combined to investigate the adsorption characteristics of NO_2 and SO_2 in M-MOF-74 (M = Mg, Zn, Ni, Co) compounds. It is found that NO_2 dissociatively adsorbs into the four compounds, forming nitrate species and nitric oxide NO as a result of disproportionation or decomposition reactions. DFT calculations predict that there is a transfer of charge from the MOF to the adsorbed NO_2, weakening the N−O bond and facilitating the dissociation reaction within the MOFs. The SO_2 molecules are found to be molecularly adsorbed into MOF-74 and have a strong binding energy (~90 kJ/mol) by establishing multipoint interactions with the MOF structure.

2. EXPERIMENTAL AND THEORETICAL METHODS

Synthesis of Mg-MOF-74, Ni-MOF-74, Co-MOF-74, and Zn-MOF-74. The MOFs samples are synthesized by following the modified procedure as described in the Supporting Information from ref 17. After thorough solvent exchange as described in ref 32, the BET surface areas reach 1078, 774, 913, and 1077 m^2/g for Mg-MOF-74, Zn-MOF-74, Ni-MOF-74, and Co-MOF-74,[32] respectively, consistent with the values reported in the original literature.[17]

Infrared Spectroscopy. A powder of the MOF-74 sample (~2 mg) was pressed onto a KBr pellet for SO_2 measurement and a tungsten mesh (~1.3 cm diameter, 1−2 mm thick) for NO_2 exposure, since NO_2 reacts with KBr. The sample was placed into a high-pressure high-temperature cell at the focal point of the sample compartment of the infrared spectrometer. The cell was connected to a vacuum line for evacuation (base pressure ~10−20 mTorr). The samples were activated by evacuation at 180 °C in vacuum (<20 mTorr) for at least 3 h, until IR measurements showed that the H_2O preadsorbed during sample preparation was fully removed (see IR spectra of activated MOFs in Figure S1). For reference, the NO_x (mainly NO and NO_2) and SO_2 concentrations in the flue gas are around 500 ppm level.[8] To increase the signal in IR absorption spectra, 3 Torr NO_2 was introduced into the pressure cell, and all spectra were recorded in transmission between 400 and 4000 cm^{-1} (4 cm^{-1} spectral resolution, sufficient for the inhomogeneous widths of >10 cm^{-1}) as a function of time. For SO_2 exposure, an even higher pressure (~20 Torr) was selected for increasing SO_2 loading, making it easier to distinguish its IR absorption peak from the perturbation of the MOFs vibrational bands located in the same spectral region (1500 to 1000 cm^{-1}). Desorption was initiated by evacuating the cell (<20 mTorr), and the spectra were then recorded as a function of time at each temperature investigated.

DFT Calculation. The *ab initio* calculations in this work were performed at the DFT level with a plane-wave basis, as implemented in the VASP code.[33,34] In order to take into account the important Van der Waals interactions, the Van der Waals density functional vdW-DF[35−38] was used, together with projector augmented pseudopotentials[34] and a plane-wave expansion for the wave functions with a cutoff energy of 600 eV. All the systems were optimized until the forces acting on each atom were smaller than 1 meV/Å. Due to the large dimensions of the unit cell, i.e. 54 atoms plus the guest molecules, only the Γ point was sampled.

3. EXPERIMENTAL RESULTS

3.1. NO_2 Adsorption into M-MOF-74 (M = Zn, Mg, Ni, Co). To examine the interaction of NO_2 with Zn-MOF-74, 3 Torr NO_2 is introduced into the Zn-MOF-74 (previously activated under vacuum), and IR spectra are recorded for 1 h with the system sealed (see Figure 1). A strong band appears at 1684 cm^{-1} and grows slowly as a function

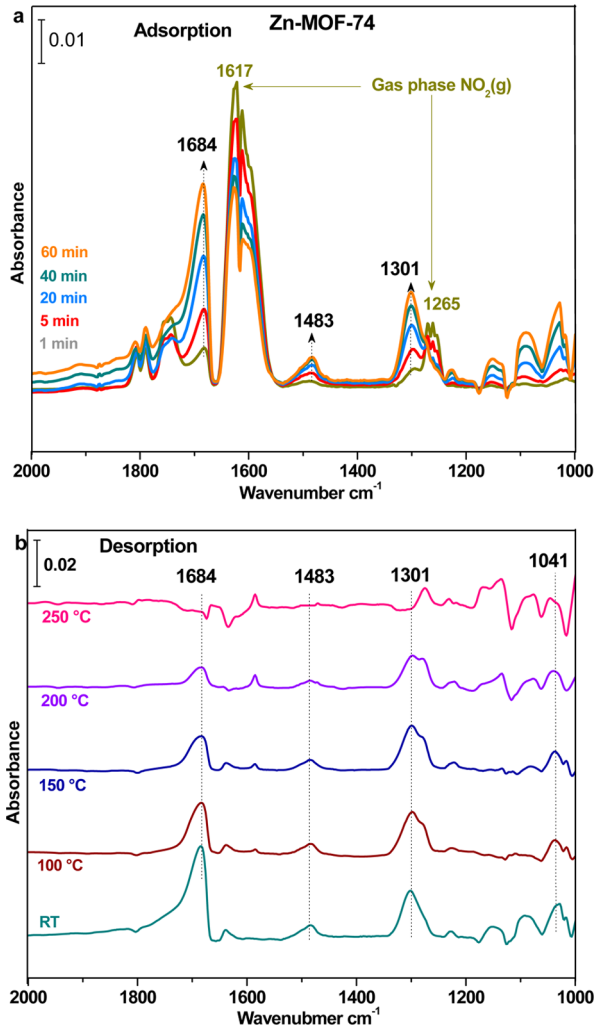

Figure 1. (a) IR absorption spectra of NO_2 adsorption into Zn-MOF-74 as a function of time under 3 Torr. (b) IR spectra of NO_x desorption from Zn-MOF-74 under vacuum as a function of temperature. The spectra are recorded at room temperature after evacuation at 24, 100, 150, 200, and 250 °C for 1 h. All the spectra are referenced to the activated (empty) MOFs in vacuum (<20 mTorr).

of time. Two other bands at 1483 and 1301 cm^{-1} also increase in intensity during the exposure. Gas phase NO with the peak center at 1874 cm^{-1} can be also detected, and its intensity increases with time. At the same time, the intensities of the gas phase NO_2 bands at 1617 and 1265 cm^{-1} decrease due to adsorption into MOFs and on the cell walls. After 60 min, the gas phase NO_2 and product NO are evacuated, and the spectra are recorded during the desorption process as a function of temperature shown in Figure 1b. The observed absorption bands at 1684, 1483, and 1301 cm^{-1} remain unchanged upon evacuation at room temperature. Above 100 °C, the band at 1684 cm^{-1} disappears. However, the bands at 1483 and 1301 substantially weaken only at 200 °C.

DOI: 10.1021/acs.chemmater.7b00005
Chem. Mater. 2017, 29, 4227−4235

Mg-, Ni-, and Co-MOF-74 are also exposed to 3 Torr NO_2 gas, and the spectra recorded during evacuation are summarized in Figure 2. Similar bands are observed at 1667, 1497, and 1303 cm^{-1} in the case of Mg-MOF-74; at 1698, 1486, and 1278 cm^{-1} in the case of Ni-MOF-74; and at 1703, 1475, and 1291 cm^{-1} in the case of Co-MOF-74. For M-MOF-74 (M = Ni, Co), exposure of NO_2 gives rise to bands at 1837 and 1801 cm^{-1} that are assigned to nitrosyl (NO) species in the discussion below.

These nitrosyl species can be easily removed at elevated temperatures (above 100 °C) from Ni- and Co-MOF-74 under evacuation. However, the other characteristic bands associated with adsorbed NO_2 are hardly affected until the sample is annealed to 200 °C. The temperature cannot be increased above 300 °C, when the frameworks undergo thermal decomposition. The perturbation of the ring C−H bending mode β(CH) in the 1120−1130 cm^{-1} region and the MOF combination mode around 1812 cm^{-1} are detected in the spectra of all compounds.[32]

3.2. SO_2 Adsorption into M-MOF-74 (M = Zn, Mg, Ni, Co). For the study of SO_2 interaction with MOF-74, the activated MOF-74 compounds are exposed to higher pressures (~20 Torr) to increase SO_2 loading and be able to distinguish its IR absorption bands from the perturbation of the MOFs phonon bands as mentioned earlier. After 30 min, the gas phase is evacuated, and IR spectra are recorded as a function of time during the desorption process as shown in Figure 3. The adsorbed SO_2 species can be well distinguished in the IR spectra by their $\nu_{as}(SO_2)$ mode above 1300 cm^{-1} and $\nu_s(SO_2)$ mode above 1100 cm^{-1}. The stretching modes are red-shifted from their gas phase values (ν_{as} 1362 cm^{-1}, ν_s 1151 cm^{-1}) in the four compounds Zn-, Mg-, Ni-, and Co-MOF-74 by 43, 38, 43, and 57 cm^{-1} for ν_{as}, respectively. For the $\nu_s(SO_2)$ mode, the frequency position appears in the range from 1100 to 1130 cm^{-1} where the perturbation of β(C−H) mode occurs, as is also observed in the case of NO_2 adsorption. Therefore, it is difficult to determine the exact frequency. In general, the frequency shifts of SO_2 in this MOF are typical for *physisorbed* species.[39,40] In addition, the β(C−H) framework mode is also strongly perturbed around 1200 cm^{-1}, for example 1236 cm^{-1} in Mg-MOF-74, indicating that there is an interaction between SO_2 and the phenyl ring. The same observation can be also made in Zn-, Ni-, and Co-MOF-74 at 1197, 1195, and 1193 cm^{-1}, respectively.

The adsorbed SO_2 species gradually desorbs from the frameworks under evacuation at room temperature and can be completely removed upon heating to the 150 °C in vacuum. In M-MOF-74 (M = Zn, Mg), there is always a notable perturbation of the MOF framework as gas or moisture is removed by evacuation (~10 to 30 mTorr), due to the extreme sensitivity of MOFs vibrational modes around 1000 to 1600 cm^{-1} to the gas loading, especially to water vapor.[41] The X-ray powder diffraction spectra in Figure S2 show that the crystalline structure of MOF-74 [M-Zn, Mg, Ni, Co] samples is retained after both NO_2 and SO_2 exposure. However, there are noticeable changes for the relative intensities of strongest peaks in each sample after NO_2 exposure, associated with the $(2\bar{1}0)$ and (300) reflection planes.

4. DISCUSSION

The spectroscopic results in Section 3 indicate that several stable species are formed after NO_2 adsorption into M-MOF-74 (M = Zn, Mg, Ni, Co) compounds. In Zn-MOF-74, the component at 1684 cm^{-1} can be gradually removed upon evacuation under mild annealing up to 100 °C, indicating that it corresponds to different adsorbed species that are characterized by absorption bands at 1483, 1301, and 1028 cm^{-1}. These bands appear at slightly different frequencies in M-MOF-74 (M = Mg, Ni, Co). These well-resolved bands are assigned to the nitrate species most likely forming bridging or chelating complexes (see Scheme 1), typical of bidentate nitrate characterized by a splitting larger than 180 cm^{-1} between the two highest frequency bands.[42] For example, in Zn-(benzothiazole)$_2$(NO$_3$)$_2$ compounds the splitting is 185 cm^{-1} between 1485 and 1300 cm^{-1} bands, which is in agreement

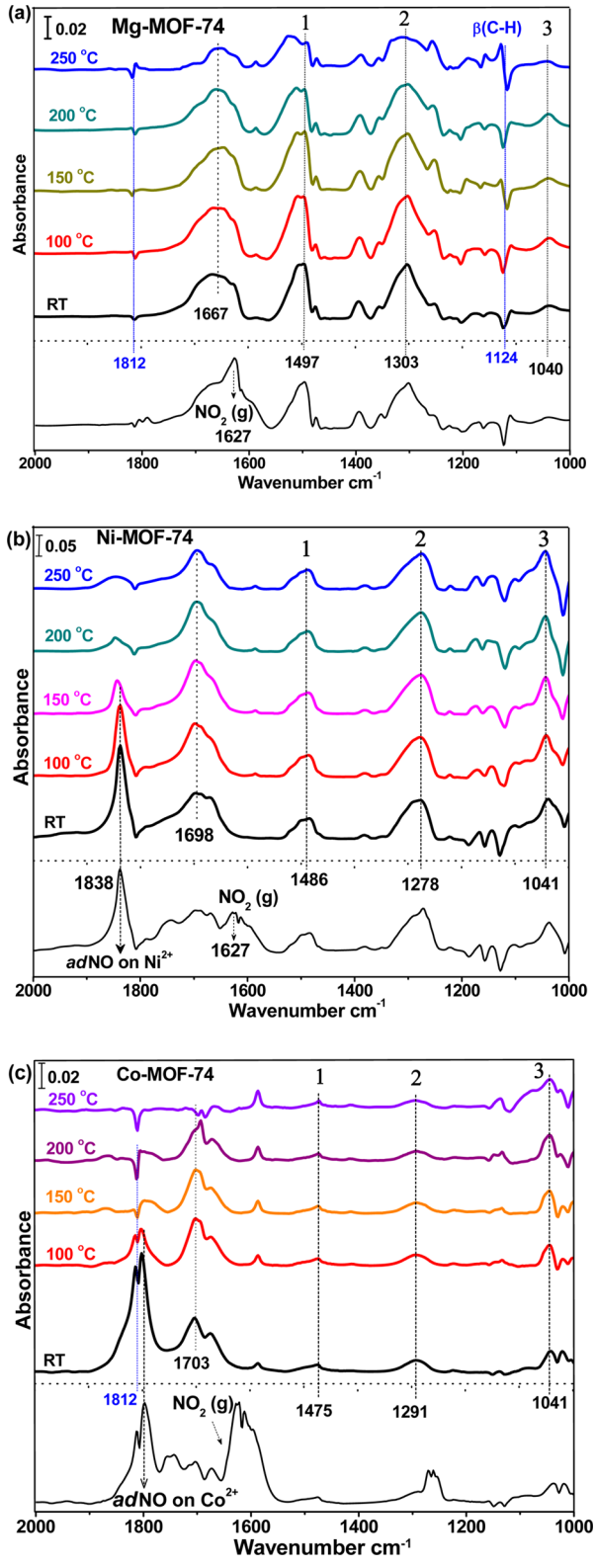

Figure 2. IR spectra of NO_x desorption from (a) Mg, (b) Ni, and (c) Co-MOF-74 under vacuum as a function of temperature after exposing to NO_2. The spectra are recorded at room temperature after evacuation at 24, 100, 150, 200, and 250 °C for 1 h, and the bottom black lines show the spectra before and after evacuation of gas phase NO_2 at room temperature. The three internal vibrations of the nitrate species are labeled as 1, 2, and 3. All the spectra are referenced to the activated (empty) MOFs in vacuum (<20 mTorr).

DOI: 10.1021/acs.chemmater.7b00005
Chem. Mater. 2017, 29, 4227−4235

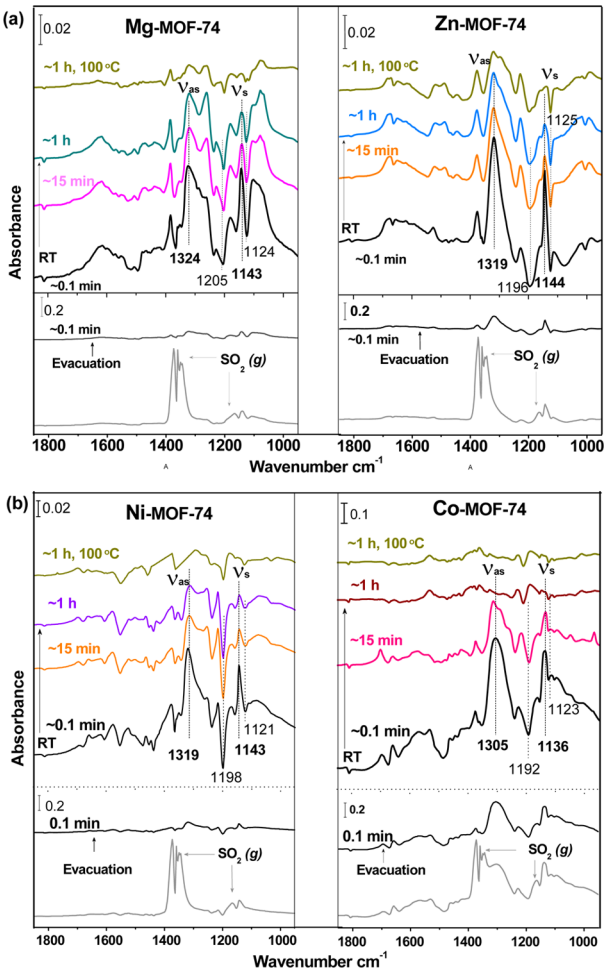

Figure 3. IR spectra of SO_2 adsorption and desorption for MOF-74 [Zn, Mg in (a) and Ni, Co in (b)] compounds. The bottom in each figure shows the gas phase SO_2 under 20 Torr (gray spectra) and the evacuation of the gas phase after 0.5 min (black spectra). The following four spectra above show the evacuation process under vacuum as a function of time at room temperature and 150 °C for 1 h. All the spectra are referenced to the activated (empty) MOFs in vacuum (<20 mTorr).

Scheme 1. Chelating Bidentate Nitrate Complex

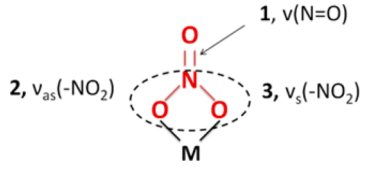

with a previous report.[42] The three bands labeled as 1, 2, and 3 in Figure 2 and Scheme 1 are assigned to the N═O stretching and the asymmetric and symmetric stretching vibrations of $-NO_2$ within NO_3^-.

The reaction product of NO_2 with MOF-74 is also quite similar to that of NO_2 adsorption on many metal oxides surfaces such as ZnO, CeO_2, CuO, BaO, and TiO_2 at room temperature.[28,30,31,43−45] The surfaces get nitrated upon exposure to NO_2 by the following reaction pathways as predicted by Rodriguez and co-workers:[28,31]

$$NO_2(ads) + M{-}O \rightarrow Mg{-}NO_3(ads) \quad (1)$$

$$2NO_2(ads) \rightarrow NO_3^-(ads) + NO(gas) \quad (2)$$

In our case, the second pathway (2) is more likely since the coexistence of NO_3^- and NO gas or nitrosyl groups is detected in the IR spectra. Figure 2 shows that NO is formed and coordinated with $Ni^{2+}$and Co^{2+} by 1:1 nitrosyl adducts after adsorption in Ni- and Co-MOF-74, suggesting that the metal center is the main reactive center for NO_2 molecules. Due to π-back-donation from d-electrons of Ni and Co to NO molecules, NO interacts strongly with the metal centers Ni^{2+} and Co^{2+} with heat of adsorption over 90 kJ/mol.[41] The absence of d-electrons in Mg^{2+} prevents NO backbonding to the metal center.[21]

The absorption bands at 1660−1700 cm^{-1} are removed at higher temperatures in Zn-MOF-74 but not in the other three compounds (Ni-, Co-, and Mg-MOF-74). These bands have also been observed in Ag-ZSM, Cu-ZSM, and Co^{2+}/SiO_2 compounds and assigned to molecularly adsorbed NO_2 with partial electron donation to the surface, resulting in a blue shift of the $\nu_{as}(NO_2)$ band.[46−49] The difference of bonding strength of this species in the different M-MOF-74 (M = Zn, Mg, Ni, Co) compounds indicates that open metal ions are the adsorption centers.

To understand the interaction of NO_2 and SO_2 with the M-MOF-74 (M = Zn, Mg, Ni, Co) compounds, and the formation of nitrate species, we compare the adsorption of NO_2 and SO_2 on metal oxide surfaces, such as MgO and ZnO. The NO_2 molecule is a radical molecule that has a large electron affinity (2.4−2.5 eV).[50] The highest occupied molecular orbital is only half occupied. This makes its bonding with occupied and empty states of metal centers such as Mg on MgO and Zn on ZnO surfaces quite possible by electron donor−acceptor interactions.[28,31] Previously, DFT calculations have shown that the bonding interaction of adsorbed NO_2 with metal sites is stronger than with the oxygen sites on metal oxide surfaces and that the interaction induces the weakening of the N−O bonds, which facilitates the dissociation of NO_2 molecules.[28,31] For example, it was observed by synchrotron-based photoemission and X-ray absorption near-edge spectroscopy (XANES) that the surfaces get nitrated after NO_2 adsorption on different types of oxides (MgO, ZnO, TiO, CeO) due to the partial decomposition or disproportionation of NO_2 adsorbed onto these surfaces.[28,30,31,43,45] SO_2 molecules are less reactive with metal sites of oxide surfaces than NO_2 molecules since the LUMO of SO_2 appears at much higher energy, close to the vacuum level,[31] than the occupied states of the metal centers such as Mg or Zn. This makes the bonding interaction between SO_2 and Mg or Zn very difficult.[31] The oxygen site is found to be the active site for SO_2 upon chemical adsorption onto the surface, with the formation of sulfite at 300 K.[27,29]

These pioneering studies on oxides suggest that the NO_2 molecules should bind more strongly to the open metal sites of MOF-74 than SO_2 molecules. However, the different chemical environments in porous MOFs compared to oxide surfaces (e.g., nanopore confinement) could lead to more complex interactions. To get a better understanding of the observed experimental results, the bonding interactions of SO_2 and NO_2 molecules with MOF have been examined using first-principles calculations.

The binding energies for loadings of one (1/6 loading) and six guest molecules (6/6 loading) were calculated using the following equation

DOI: 10.1021/acs.chemmater.7b00005
Chem. Mater. 2017, 29, 4227−4235

$$E_B = (E[\mathrm{MOF}{+}n{\cdot}\mathrm{X}] - E[\mathrm{MOF}] - n{\cdot}E[\mathrm{X}])/n \quad (3)$$

where X = SO_2 or NO_2 is the molecule being adsorbed in the MOF, n is the number of adsorbed molecules, E[MOF+n·X] is the energy of the MOF with the n·X molecules adsorbed on the metal sites, E[MOF] is the energy of the MOF alone, and E[X] is the energy of the isolated molecule X. It is important to note that in eq 3 a negative binding energy denotes favorable adsorption. In parallel, an incremental binding energy is also defined, i.e., the energy of a second molecule adsorbed (2/6 loading), as

$$E_{B(2/6)} = E[\mathrm{MOF}{+}2{\cdot}\mathrm{X}] - E[\mathrm{MOF} + \mathrm{X}] - E[\mathrm{X}] \quad (4)$$

The adsorption of molecules at the metal site in MOF can give rise to electron transfer phenomena, with a net redistribution of electronic charge density from the molecule to the MOF or vice versa. To assess the valence charge density redistribution we computed the $\Delta\rho$ as defined in eq 5

$$\Delta\rho = \rho_{\mathrm{MOF+X}} - \rho_{\mathrm{X}} - \rho_{\mathrm{MOF}} \quad (5)$$

where $\rho_{\mathrm{MOF+X}}$ is the charge density of the MOF with the adsorbed molecule, and ρ_{X} denotes the charge density of the insolated molecule at the exact position and geometry as adsorbed on the MOF. ρ_{MOF} is the valence charge density of the MOF without the guest molecule. MOF-74 offers several potential binding sites associated with the nature of their building blocks. However, their potential energy surface (PES) is complex, presenting many adsorptions "pockets". In general, it has been demonstrated that the most reactive sites are uncoordinated metal centers such as Zn^{2+}, Mg^{2+}, Ni^{2+}, and Co^{2+} in MOF-74.

4.1. NO_2 Adsorption into Zn-MOF-74. Rodriguez and co-workers[31] have shown that both metal Zn and oxide ZnO surfaces exhibit a strong reactivity toward NO_2 molecules. After the adsorption of nitrogen dioxide, N, O, NO, and NO_3^-, species are found on the Zn and ZnO surfaces. Therefore, this work focuses on the interaction of the nitrogen dioxide with the metal centers of the Zn-MOF-74 to elucidate the origin of NO_2 dissociation. The reaction products are quite similar in the four MOF compounds. We believe that our analysis obtained on Zn-MOF-74 can be applied to the other three M-MOF-74 (M = Mg, Ni, Co). Previous studies only examined the bonding configuration of NO_2 to the MOF structure via one oxygen atom of NO_2 on top of the metal sites.[21] In the present calculations, three different configurations for the adsorption of the NO_2 molecule were considered on the basis of the tested adsorption geometries on metal oxide such as ZnO, MgO, and TiO_2,[28,31,45] these are *a*) the N atom of the NO_2 molecule directly interacts with the metal ion of the MOF, *b*) one of the O atoms of the NO_2 molecule interacts with the metal ion of the MOF, and *c*) the two O atoms of the NO_2 molecule interact with the metal ion of the MOF. Panels a), b), and c) of Figure 4 show the three adsorption geometries.

Table 1 shows the adsorption energies and the distances between the NO_2 molecule (the N or O depending on the adsorption configuration) and the metal ion of the MOF. This was done for loadings of one (1/6) and two (2/6) molecules per unit cell. From this table, it can be seen that the configurations *b*) and *c*) (panels b) and c)) of Figure 4 are the most stable. The NO_2 molecules have a stronger adsorption on the Zn-MOF-74 than the SO_2 molecules, as can be seen from Tables 1 and 2. From Table 1 it can be seen that the distance between the NO_2 molecule and the Zn atom decreases as the adsorption energy progressively increases. In general, the geometry of the nitrogen dioxide molecule is highly perturbed upon adsorption. However, the bond lengths of the NO_2 molecule are elongated only for the adsorption configurations

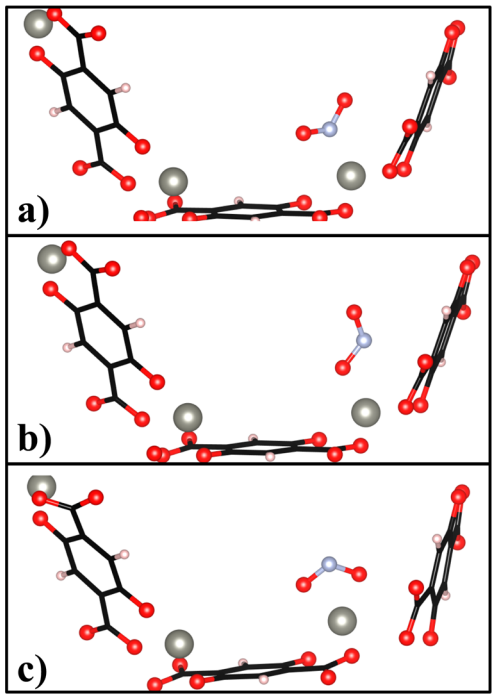

Figure 4. NO_2 adsorption geometries: red, white, light blue, and gray spheres represent O, H, N, and Zn atoms, respectively. C atoms are not shown. The geometries are denoted as NO_2 adsorption configurations a), b), and c).

Table 1. Adsorption Energies, Distances between N or O (Depending on the Adsorption Configuration) and the Metal Center of the MOF, and Bond Lengths of the NO_2 Molecule[a]

model	loading	ΔE (kJ mol^{-1})	NO_2—M (Å)	N–O bond length 1 (Å)	N–O bond length 2 (Å)
Zn–N(a)	1/6	−61.03	2.18	1.25	1.25
Zn–N(a)	2/6	−67.55	2.15	1.25	1.25
Zn–O(*b*)	1/6	−70.26	2.11	1.30	1.23
Zn–O(*b*)	2/6	−95.91	2.03	1.33	1.22
Zn–O(*c*)	1/6	−99.48	2.16	1.29	1.28
Zn–O(*c*)	2/6	−113.71	2.16	1.28	1.28
NO_2 molecule	1/6			1.22	1.22

[a]The column labeled as "bond length 1" denotes the guest molecule bond length which is closer to the metal center of the MOF, while the last column refers to the second bond length.

Table 2. Charge Gained by the Atoms of the NO_2 Molecule upon Adsorption[a]

model (1/6 loading)	charge gained by N (e)	charge gained by O (e)	charge gained by O (e)	net charge gained be the NO_2 molecule (e)
Zn–N (a)	0.199	0.154	0.138	0.491
Zn–O(b)	0.016	0.278	0.162	0.456
Zn–O(*c*)	-0.006	0.361	0.351	0.706

[a]The third column corresponds to the O atom that is closer to the metal ion of the MOF, while the fourth column refers to the other O atom.

DOI: 10.1021/acs.chemmater.7b00005
Chem. Mater. 2017, 29, 4227−4235

b) and *c*) where the O atoms directly interact with the metal center. For the geometry depicted in panel a) of Figure 4, the elongation of the NO_2 molecule is almost negligible, see Table 1.

In order to understand the perturbation of the guest molecule, we have used eq 5 to calculate the redistribution of valence charge density in the system upon adsorption of the NO_2 molecule, and this is shown in Figure 5. From Figure 5 it

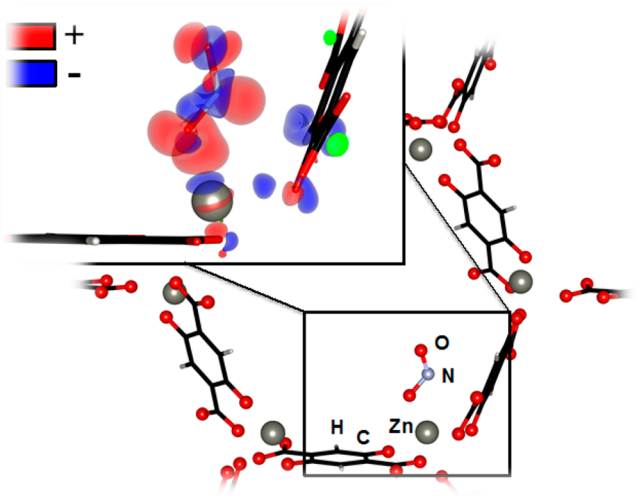

Figure 5. Redistribution of valence charge density upon adsorption of the NO_2 molecule in the Zn-MOF-74 system. The blue and red colors denote depletion and excess of charge, respectively. The iso-surface level was set to 0.018 e/Å^3.

is clear that there is a net charge transfer between NO_2 and open Zn sites. A qualitative charge analysis (using the Bader charges) of the configuration of Figure 5 reveals that the Zn atom experiences a depletion of ~0.063 *e*. On the other hand, for the NO_2 molecule the O interacting with the Zn experiences an increase of 0.278 *e*, while the second O experiences an increase of 0.162 *e*. Similar results have been obtained for the adsorption configurations a) and c) (see also Table 2). In Table 2, the NO_2 molecule experiences a gain in charge upon adsorption for all the adsorption configurations studied here. Unsurprisingly, the charge uptake by the O atoms is proportional to the elongation of the O−N bond (see Tables 1 and 2). This makes the adsorption configurations b) and c) ideal precursors for dissociation and formation of other nitrate species by the disproportionation reaction:

$$NO_2(gas) + M^{2+} \rightarrow M^{2+}{-}O + NO(gas) \quad (6)$$

$$NO_2(gas) + M^{2+}{-}O \rightarrow M^{2+}{-}NO_3 \quad (7)$$

In conclusion, the NO_2 molecule experiences a weakening in the O−N bond for the adsorption configurations b) and c) due to the valence charge redistribution upon adsorption. This weakening of the O−N bond facilitates the splitting of the molecule, explaining the experimentally observed nitrate species at room temperature. Rodrigez and co-workers[45] have found similar results for the interaction of NO_2 with a TiO_2(110) single crystal and powders of titania, where the elongation of the O−N bond facilitates the dissociation of the adsorbate.

4.2. SO_2 Adsorption into M-MOF-74 (M = Mg, Zn). To guide the construction of initial and realistic adsorption geometries, we initially assumed that the interaction of SO_2 with the MOF structure was similar to what occurs when SO_2 is adsorbed on simpler systems such MgO and ZnO surfaces. This assumption is fully justified since the oxygen atoms surrounding the metals sites of M-MOF-74 "recreate" the chemical environment found on these oxide surfaces. Theoretical and experimental evidence of the adsorption of SO_2 on MgO and ZnO surfaces suggests that SO_2 interacts favorably with the metal species exposed at the surface through its oxygen atoms. Although interaction with the sulfur atom is less likely, we have also considered this option here. Starting from these qualitative considerations, we examine the adsorption geometry of SO_2 in the MOF structure to maximize its interaction with the metal sites, which are expected to be the most reactive binding centers.

For MOF-74, we explored two types of interaction of SO_2 with the metal sites: *i*) when one of the oxygen atoms of SO_2 interacts with the metal ions (i.e., Mg or Zn) and *ii*) when the sulfur binds to the exposed metal sites. However, the calculations indicate that, when a SO_2 molecule is placed in M-MOF-74 (M = Zn, Mg) according to case *ii*), the structural optimization leads to case *i*). We have investigated the effect of loading and therefore the extent of lateral interactions in the final absorption properties from one molecule (low-loading) up to six SO_2 (high-loading).[51] Table 3 shows the adsorption energies together with the relative contribution for these cases.

Table 3. Adsorption Energies ΔE (in kJ/mol) of SO_2 in M-MOF-74 (M = Mg, Zn)[a]

model	loading	ΔE	ΔE_{ZPE}	ΔH_{298}	O−M
MOF-74-Mg					
Mg−O	1/6	−91	−88	−91	2.14
Mg−O	6/6	−90	−87	−90	2.17
MOF-74-Zn					
Zn−O	1/6	−72	−70	−73	2.20

[a]ΔE (in kJ/mol) is also given, corrected by the ZPE and thermal contribution ΔH at 298 K (in kJ/mol). O−M are the averaged intermolecular bond length OSO−M-(MOF-74) in Å.

The binding energies in Table 3 suggest that SO_2 establishes strong interactions with the unsaturated metal centers of M-MOF-74 (M = Zn, Mg). This is further validated by isotherm measurements of SO_2 in Mg-MOF-74 in which the uptake reaches up to 8.60 mmol/g at 1.02 bar (see adsorption data in Figure S3), which is significantly higher than the CO_2 uptake (6.18 mmol/g) in Mg-MOF-74 under the same condition since the latter binds more weakly (47 kJ/mol).[18] In Zn-MOF-74, a low loading situation is considered only, i.e., one molecule per cell. Note that Mg-MOF-74 has a larger affinity for SO_2 than the iso-structural Zn-MOF-74. Our findings are in agreement with the early computational studies of the adsorption of SO_2 on MgO and ZnO surfaces (87.9 kJ/mol for MgO and 66.9 kJ/mol for ZnO).[27,29] Table 3 also suggests that low loading is more favorable than high-loading, due to the repulsion between adsorbed SO_2 molecules. This effect is clearly manifested in an increase of the bond-length between O and the metal site in high-loading situations. A similar effect has been shown previously for H_2O in Mg-MOF-74.[52]

Furthermore, examination of the local adsorption geometry of SO_2 in M-MOF-74 (M = Mg, Zn) reveals multipoint interactions between SO_2 and the MOF structure: one oxygen atom (of SO_2) engages the metal site (Mg or Zn) and establishes the primary interaction with MOFs, whereas the

DOI: 10.1021/acs.chemmater.7b00005
Chem. Mater. 2017, 29, 4227−4235

sulfur atom also interacts directly with one of the oxygen atoms of the linker (see Figure 6), increasing the binding energy.

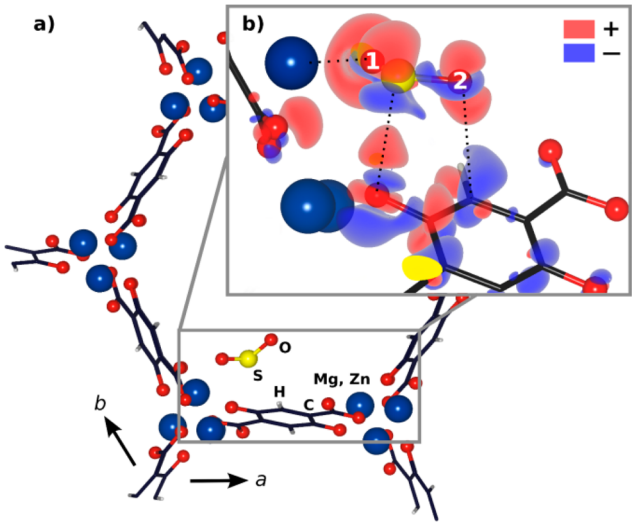

Figure 6. (a) M-MOF-74 (M = Mg, Zn) in contact with SO_2, (b) enlargement of the adsorption area, also showing charge density differences, $\Delta\rho$ (eq 5), only for Mg-MOF-74. Color scheme: blue = Mg or Zn; red = oxygen; black = carbon; white = hydrogen; yellow = sulfur. Dashed lines highlight relevant interactions (i.e., O(1)−Mg, S−O, and O(2)−C) of the molecule with the MOF. Red density lobes represent areas where charge density was added, whereas blue represents that charge was removed. The iso-surface level was set to 0.018 e/Å^3.

We have investigated how the valence charge density of Mg-MOF-74 and SO_2 is redistributed after molecular adsorption, using eq 5. Figure 7 shows a large redistribution of the valence

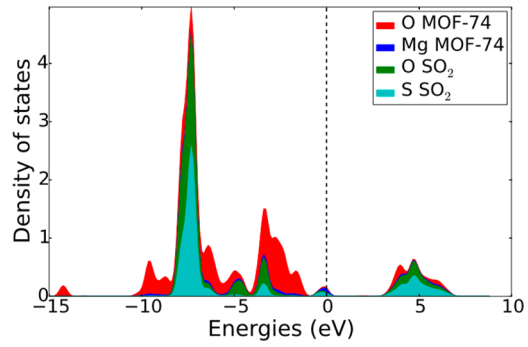

Figure 7. Local density of states (LDOS) of the Mg-MOF-74 with adsorbed SO_2 onto the open metal sites. The Fermi energy is aligned at the zero level of the horizontal axis.

charge density: the oxygen atom connected to the benzene donates some charges, giving rise to its interactions with the S atom. One of the oxygen atoms of SO_2 (label 1 in panel b of Figure 6) engages the Mg of the MOF (not shown for clarity), while the other interacts (label 2 in panel b of Figure 6) with a carbon atom in the benzene ring, which also experiences a charge redistribution and polarization. Figure 6 displays the calculated density of states for the occupied bands in Mg-MOF-74+SO_2. Both S and O states coming from SO_2 overlap with Mg and O bands of the MOF. However, the overlapping of O of SO_2 with the MOF states is more than S, reflecting the type of binding between SO_2 and MOFs. The interaction of SO_2 with Zn-MOF-74 is similar but weaker. The large adsorption energy is therefore the result of the three-interactions established by the three atoms of SO_2 with MOF-74.

5. CONCLUSIONS

In summary, the spectroscopic results give insight into the adsorption behaviors of flue gas contaminants NO_2 and SO_2 in M-MOF-74 (M = Zn, Mg, Ni, Co) compounds at room temperature. NO_2 exhibits a rich chemistry in all four compounds. After NO_2 adsorption, molecular adsorbed NO_2 appears around 1660−1700 cm^{-1} in IR spectra, and nitrate and nitric oxide species are also formed due to decomposition reactions and remain stable at higher temperature (>150 °C). DFT calculations show that a strong NO_2−Zn bonding interaction induces a significant weakening of the N−O bond, facilitating the decomposition of the NO_2 molecules. SO_2 is strongly adsorbed into MOF-74 with a binding energy (>90 kJ/mol for Mg-MOF-74 and >70 kJ/mol for Zn-MOF-74), higher than that of CO_2 (40 to 50 kJ/mol). DFT calculations further suggest multipoint interactions between SO_2 molecules and MOFs. Finally, our IR results show that adsorbed SO_2 can be removed upon annealing to 150 °C. Preadsorption of these molecules could poison the open metal sites and therefore lead to the significant decrease of CO_2 uptake. These findings suggest that denitrification ($DeNO_x$) processes and desulfurization ($DeSO_x$) are needed for using MOF-74 materials as carbon capture medium in flue gas applications.

■ ASSOCIATED CONTENT

Supporting Information

The Supporting Information is available free of charge on the ACS Publications website at DOI: 10.1021/acs.chemmater.7b00005.

Sample preparation and activation methods; IR spectra of MOFs samples; powder X-ray diffraction pattern of MOFs samples; isotherm measurement of SO_2 adsorption into Mg-MOF-74 (PDF)

■ AUTHOR INFORMATION

Corresponding Author

*E-mail: chabal@utdallas.edu.

ORCID

Kui Tan: 0000-0002-5167-7295

Pieremanuele Canepa: 0000-0002-5168-9253

Jing Li: 0000-0001-7792-4322

Notes

The authors declare no competing financial interest.

■ ACKNOWLEDGMENTS

This work was entirely supported by the Department of Energy Grant No. DE-FG02-08ER46491. T.T. also acknowledges generous support from the Simons Foundation through Grant No. 391888, which endowed his sabbatical leave at MIT.

■ REFERENCES

(1) Chen, B. L.; Eddaoudi, M.; Hyde, S. T.; O'Keeffe, M.; Yaghi, O. M. Interwoven metal-organic framework on a periodic minimal surface with extra-large pores. *Science* **2001**, *291*, 1021−1023.

(2) Eddaoudi, M.; Li, H. L.; Yaghi, O. M. Highly porous and stable metal-organic frameworks: Structure design and sorption properties. *J. Am. Chem. Soc.* **2000**, *122*, 1391−1397.

DOI: 10.1021/acs.chemmater.7b00005
Chem. Mater. 2017, 29, 4227−4235

(3) Rosi, N. L.; Eckert, J.; Eddaoudi, M.; Vodak, D. T.; Kim, J.; O'Keeffe, M.; Yaghi, O. M. Hydrogen storage in microporous metal-organic frameworks. *Science* **2003**, *300*, 1127−1129.
(4) Eddaoudi, M.; Kim, J.; Rosi, N.; Vodak, D.; Wachter, J.; O'Keefe, M.; Yaghi, O. M. Systematic design of pore size and functionality in isoreticular MOFs and their application in methane storage. *Science* **2002**, *295*, 469−472.
(5) Wu, H.; Zhou, W.; Yildirim, T. High-Capacity Methane Storage in Metal Organic Frameworks M_2(dhtp): The Important Role of Open Metal Sites. *J. Am. Chem. Soc.* **2009**, *131*, 4995−5000.
(6) Low, J. J.; Benin, A. I.; Jakubczak, P.; Abrahamian, J. F.; Faheem, S. A.; Willis, R. R. Virtual High Throughput Screening Confirmed Experimentally: Porous Coordination Polymer Hydration. *J. Am. Chem. Soc.* **2009**, *131*, 15834−15842.
(7) Li, J.-R.; Sculley, J.; Zhou, H.-C. Metal−Organic Frameworks for Separations. *Chem. Rev.* **2012**, *112*, 869−932.
(8) Sumida, K.; Rogow, D. L.; Mason, J. A.; McDonald, T. M.; Bloch, E. D.; Herm, Z. R.; Bae, T.-H.; Long, J. R. Carbon Dioxide Capture in Metal−Organic Frameworks. *Chem. Rev.* **2012**, *112*, 724−781.
(9) Getman, R. B.; Bae, Y.-S.; Wilmer, C. E.; Snurr, R. Q. Review and Analysis of Molecular Simulations of Methane, Hydrogen, and Acetylene Storage in Metal−Organic Frameworks. *Chem. Rev.* **2012**, *112*, 703−723.
(10) Simmons, J. M.; Wu, H.; Zhou, W.; Yildirim, T. Carbon capture in metal-organic frameworks-a comparative study. *Energy Environ. Sci.* **2011**, *4*, 2177−2185.
(11) Arstad, B.; Fjellvåg, H.; Kongshaug, K.; Swang, O.; Blom, R. Amine functionalised metal organic frameworks (MOFs) as adsorbents for carbon dioxide. *Adsorption* **2008**, *14*, 755−762.
(12) Vaidhyanathan, R.; Iremonger, S. S.; Dawson, K. W.; Shimizu, G. K. H. An amine-functionalized metal organic framework for preferential CO2 adsorption at low pressures. *Chem. Commun.* **2009**, 5230−5232.
(13) Stavitski, E.; Pidko, E. A.; Couck, S.; Remy, T.; Hensen, E. J. M.; Weckhuysen, B. M.; Denayer, J.; Gascon, J.; Kapteijn, F. Complexity behind CO2 Capture on NH2-MIL-53(Al). *Langmuir* **2011**, *27*, 3970−3976.
(14) Zhao, Y.; Wu, H.; Emge, T. J.; Gong, Q.; Nijem, N.; Chabal, Y. J.; Kong, L.; Langreth, D. C.; Liu, H.; Zeng, H.; Li, J. Enhancing Gas Adsorption and Separation Capacity through Ligand Functionalization of Microporous Metal−Organic Framework Structures. *Chem. - Eur. J.* **2011**, *17*, 5101−5109.
(15) Liu, H.; Zhao, Y.; Zhang, Z.; Nijem, N.; Chabal, Y. J.; Zeng, H.; Li, J. The Effect of Methyl Functionalization on Microporous Metal-Organic Frameworks' Capacity and Binding Energy for Carbon Dioxide Adsorption. *Adv. Funct. Mater.* **2011**, *21*, 4754−4762.
(16) Wu, H.; Reali, R. S.; Smith, D. A.; Trachtenberg, M. C.; Li, J. Highly Selective CO2 Capture by a Flexible Microporous Metal−Organic Framework (MMOF) Material. *Chem. - Eur. J.* **2010**, *16*, 13951−13954.
(17) Caskey, S. R.; Wong-Foy, A. G.; Matzger, A. J. Dramatic Tuning of Carbon Dioxide Uptake via Metal Substitution in a Coordination Polymer with Cylindrical Pores. *J. Am. Chem. Soc.* **2008**, *130*, 10870−10871.
(18) Yazaydın, A. O. z. r.; Snurr, R. Q.; Park, T.-H.; Koh, K.; Liu, J.; LeVan, M. D.; Benin, A. I.; Jakubczak, P.; Lanuza, M.; Galloway, D. B.; Low, J. J.; Willis, R. R. Screening of Metal−Organic Frameworks for Carbon Dioxide Capture from Flue Gas Using a Combined Experimental and Modeling Approach. *J. Am. Chem. Soc.* **2009**, *131*, 18198−18199.
(19) Britt, D.; Furukawa, H.; Wang, B.; Glover, T. G.; Yaghi, O. M. Highly efficient separation of carbon dioxide by a metal-organic framework replete with open metal sites. *Proc. Natl. Acad. Sci. U. S. A.* **2009**, *106*, 20637−20640.
(20) Dietzel, P. D. C.; Johnsen, R. E.; Fjellvag, H.; Bordiga, S.; Groppo, E.; Chavan, S.; Blom, R. Adsorption properties and structure of CO_2 adsorbed on open coordination sites of metal-organic framework Ni_2(dhtp) from gas adsorption, IR spectroscopy and X-ray diffraction. *Chem. Commun.* **2008**, 5125−5127.
(21) Yu, K.; Kiesling, K.; Schmidt, J. R. Trace Flue Gas Contaminants Poison Coordinatively Unsaturated Metal−Organic Frameworks: Implications for CO_2 Adsorption and Separation. *J. Phys. Chem. C* **2012**, *116*, 20480−20488.
(22) Ding, L.; Yazaydin, A. Ö. How Well Do Metal−Organic Frameworks Tolerate Flue Gas Impurities? *J. Phys. Chem. C* **2012**, *116*, 22987−22991.
(23) Yu, J.; Balbuena, P. B. Water Effects on Postcombustion CO_2 Capture in Mg-MOF-74. *J. Phys. Chem. C* **2013**, *117*, 3383−3388.
(24) Yu, J.; Ma, Y.; Balbuena, P. B. Evaluation of the Impact of H_2O, O_2, and SO_2 on Postcombustion CO_2 Capture in Metal−Organic Frameworks. *Langmuir* **2012**, *28*, 8064−8071.
(25) Yu, K.; Schmidt, J. R. Comment on "How Well Do Metal−Organic Frameworks Tolerate Flue Gas Impurities? *J. Phys. Chem. C* **2013**, *117*, 3192−3192.
(26) Lee, K.; Howe, J. D.; Lin, L.-C.; Smit, B.; Neaton, J. B. Small-Molecule Adsorption in Open-Site Metal−Organic Frameworks: A Systematic Density Functional Theory Study for Rational Design. *Chem. Mater.* **2015**, *27*, 668−678.
(27) Rodriguez, J. A.; Jirsak, T.; Freitag, A.; Larese, J. Z.; Maiti, A. Interaction of SO_2 with MgO(100) and Cu/MgO(100): Decomposition Reactions and the Formation of SO_3 and SO_4. *J. Phys. Chem. B* **2000**, *104*, 7439−7448.
(28) Rodriguez, J. A.; Jirsak, T.; Sambasivan, S.; Fischer, D.; Maiti, A. Chemistry of NO_2 on CeO_2 and MgO: Experimental and theoretical studies on the formation of NO_3. *J. Chem. Phys.* **2000**, *112*, 9929−9939.
(29) Chaturvedi, S.; Rodriguez, J. A.; Jirsak, T.; Hrbek, J. Surface Chemistry of SO_2 on Zn and ZnO: Photoemission and Molecular Orbital Studies. *J. Phys. Chem. B* **1998**, *102*, 7033−7043.
(30) Rodriguez, J. A.; Jirsak, T.; Chaturvedi, S.; Dvorak, J. Chemistry of SO_2 and NO_2 on ZnO(0001)-Zn and ZnO powders: changes in reactivity with surface structure and composition. *J. Mol. Catal. A: Chem.* **2001**, *167*, 47−57.
(31) Rodriguez, J. A.; Jirsak, T.; Dvorak, J.; Sambasivan, S.; Fischer, D. Reaction of NO2 with Zn and ZnO: Photoemission, XANES, and Density Functional Studies on the Formation of NO3. *J. Phys. Chem. B* **2000**, *104*, 319−328.
(32) Tan, K.; Zuluaga, S.; Gong, Q.; Canepa, P.; Wang, H.; Li, J.; Chabal, Y. J.; Thonhauser, T. Water Reaction Mechanism in Metal Organic Frameworks with Coordinatively Unsaturated Metal Ions: MOF-74. *Chem. Mater.* **2014**, *26*, 6886−6895.
(33) Kresse, G.; Furthmüller, J. Efficient iterative schemes for ab initio total-energy calculations using a plane-wave basis set. *Phys. Rev. B: Condens. Matter Mater. Phys.* **1996**, *54*, 11169−11186.
(34) Kresse, G.; Joubert, D. From ultrasoft pseudopotentials to the projector augmented-wave method. *Phys. Rev. B: Condens. Matter Mater. Phys.* **1999**, *59*, 1758−1775.
(35) Langreth, D. C.; Lundqvist, B. I.; Chakarova-Kack, S. D.; Cooper, V. R.; Dion, M.; Hyldgaard, P.; Kelkkanen, A.; Kleis, J.; Kong, L.; Li, S.; Moses, P. G.; Murray, E.; Puzder, A.; Rydberg, H.; Schroder, E.; Thonhauser, T. A density functional for sparse matter. *J. Phys.: Condens. Matter* **2009**, *21*, 084203.
(36) Thonhauser, T.; Cooper, V. R.; Li, S.; Puzder, A.; Hyldgaard, P.; Langreth, D. C. Van der Waals density functional: Self-consistent potential and the nature of the van der Waals bond. *Phys. Rev. B: Condens. Matter Mater. Phys.* **2007**, *76*, 125112.
(37) Thonhauser, T.; Zuluaga, S.; Arter, C. A.; Berland, K.; Schröder, E.; Hyldgaard, P. Spin Signature of Nonlocal Correlation Binding in Metal-Organic Frameworks. *Phys. Rev. Lett.* **2015**, *115*, 136402.
(38) Berland, K.; Cooper, V. R.; Lee, K.; Schröder, E.; Thonhauser, T.; Hyldgaard, P.; Lundqvist, B. I. van der Waals forces in density functional theory: a review of the vdW-DF method. *Rep. Prog. Phys.* **2015**, *78*, 066501.
(39) Waqif, M.; Saad, A. M.; Bensitel, M.; Bachelier, J.; Saur, O.; Lavalley, J.-C. Comparative study of SO2 adsorption on metal oxides. *J. Chem. Soc., Faraday Trans.* **1992**, *88*, 2931−2936.
(40) Goodman, A. L.; Li, P.; Usher, C. R.; Grassian, V. H. Heterogeneous Uptake of Sulfur Dioxide On Aluminum and

DOI: 10.1021/acs.chemmater.7b00005
Chem. Mater. 2017, 29, 4227−4235

Magnesium Oxide Particles. *J. Phys. Chem. A* **2001**, *105* (25), 6109−6120.
(41) Bonino, F.; Chavan, S.; Vitillo, J. G.; Groppo, E.; Agostini, G.; Lamberti, C.; Dietzel, P. D. C.; Prestipino, C.; Bordiga, S. Local Structure of CPO-27-Ni Metallorganic Framework upon Dehydration and Coordination of NO. *Chem. Mater.* **2008**, *20*, 4957−4968.
(42) Nakamoto, K. *Infrared and Raman Spectra of Inorganic and Coordination Compounds*, 6th ed.; Wiley & Sons, Inc.: Hoboken, New Jersey, United States, 2009.
(43) Valyon, J.; Hall, W. K. Studies of the surface species formed from nitric oxide on copper zeolites. *J. Phys. Chem.* **1993**, *97*, 1204−1212.
(44) Broqvist, P.; Grönbeck, H.; Fridell, E.; Panas, I. Characterization of NO_x Species Adsorbed on BaO: Experiment and Theory. *J. Phys. Chem. B* **2004**, *108*, 3523−3530.
(45) Rodriguez, J. A.; Jirsak, T.; Liu, G.; Hrbek, J.; Dvorak, J.; Maiti, A. Chemistry of NO_2 on Oxide Surfaces: Formation of NO_3 on TiO_2(110) and NO_2↔O Vacancy Interactions. *J. Am. Chem. Soc.* **2001**, *123*, 9597−9605.
(46) Hadjiivanov, K. I. Identification of Neutral and Charged N_xO_y Surface Species by IR Spectroscopy. *Catal. Rev.: Sci. Eng.* **2000**, *42*, 71−144.
(47) Hadjiivanov, K. I. IR study of CO and NO_2 sorption on Ag-ZSM-5. *Microporous Mesoporous Mater.* **1998**, *24*, 41−49.
(48) Hadjiivanov, K.; Klissurski, D.; Ramis, G.; Busca, G. Fourier transform IR study of NOx adsorption on a CuZSM-5 DeNOx catalyst. *Appl. Catal., B* **1996**, *7*, 251−267.
(49) Djonev, B.; Tsyntsarski, B.; Klissurski, D.; Hadjiivanov, K. IR spectroscopic study of NOadsorption and NO-O_2 coadsorption on Co^{2+}/SiO_2catalysts. *J. Chem. Soc., Faraday Trans.* **1997**, *93*, 4055−4063.
(50) Brundle, C. R.; Neumann, D.; Price, W. C.; Evans, D.; Potts, A. W.; Streets, D. G. Electronic Structure of NO_2 Studied by Photoelectron and Vacuum-uv Spectroscopy and Gaussian Orbital Calculations. *J. Chem. Phys.* **1970**, *53*, 705−715.
(51) Nijem, N.; Pieremanuele, C.; Lingzhu, K.; Haohan, W.; Jing, L.; Timo, T.; Yves, J. C. Spectroscopic characterization of van der Waals interactions in a metal organic framework with unsaturated metal centers: MOF-74−Mg. *J. Phys.: Condens. Matter* **2012**, *24*, 424203.
(52) Canepa, P.; Nijem, N.; Chabal, Y. J.; Thonhauser, T. Diffusion of Small Molecules in Metal Organic Framework Materials. *Phys. Rev. Lett.* **2013**, *110*, 026102.

DOI: 10.1021/acs.chemmater.7b00005
Chem. Mater. 2017, 29, 4227−4235